Total alkaloids from Alstonia scholaris inhibit influenza A virus replication and lung immunopathology by regulating the innate immune response

Hong-Xia Zhou , Run-Feng Li , Yi-Feng Wang , Li-Han Shen , Li-Hua Cai , Yun-Ceng Weng , Xin-Xin Chen , Xiao Wu , Rui-Feng Chen , Hai-Ming Jiang , Caiyun Wang , Mingrong Yang , Jingguang Lu , Xiao-Dong Luo , Zhihong Jiang , Zi-Feng Yang

PII: S0944-7113(20)30103-3
DOI: https://doi.org/10.1016/j.phymed.2020.153272
Reference: PHYMED 153272

To appear in: *Phytomedicine*

Received date: 12 February 2020
Revised date: 1 June 2020
Accepted date: 28 June 2020

Please cite this article as: Hong-Xia Zhou , Run-Feng Li , Yi-Feng Wang , Li-Han Shen , Li-Hua Cai , Yun-Ceng Weng , Xin-Xin Chen , Xiao Wu , Rui-Feng Chen , Hai-Ming Jiang , Caiyun Wang , Mingrong Yang , Jingguang Lu , Xiao-Dong Luo , Zhihong Jiang , Zi-Feng Yang , Total alkaloids from Alstonia scholaris inhibit influenza A virus replication and lung immunopathology by regulating the innate immune response, *Phytomedicine* (2020), doi: https://doi.org/10.1016/j.phymed.2020.153272

Total alkaloids from *Alstonia scholaris* inhibit influenza A virus replication and lung immunopathology by regulating the innate immune response

Hong-Xia Zhou[a, #], Run-Feng Li[a, #], Yi-Feng Wang[b], Li-Han Shen[c], Li-Hua Cai[c], Yun-Ceng Weng[a], Xin-Xin Chen[a], Xiao Wu[a], Rui-Feng Chen[a], Hai-Ming Jiang[a], Caiyun Wang[d], Mingrong Yang[d], Jingguang Lu[d], Xiao−Dong Luo[a,b,*], Zhihong Jiang[a,d,f *], Zi-Feng Yang[a,d,e,f*]

[a] *State Key Laboratory of Respiratory Disease, National Clinical Research Center for Respiratory Disease, Guangzhou Institute of Respiratory Health, the First Affiliated Hospital of Guangzhou Medical University, Guangzhou Medical University, Guangzhou, Guangdong, 510120, China*

[b] *State Key Laboratory of Phytochemistry and Plant Resources in West China, Kunming Institute of Botany, Chinese Academy of Sciences, Kunming, 650201, China*

[c] *Dongguan People's Hospital, Dongguan, 523000, China*

[d] *State Key Laboratory of Quality Research in Chinese Medicine, Macau University of Science and Technology, Macau (SAR), 519020, China*

[e] *KingMed Virology Diagnostic & Translational Center, 510000, China*

[f] *Guangdong-Hong Kong-Macao Joint Laboratory of Infectious Respiratory Disease, 510000, China*

[#] Hongxia Zhou and Runfeng Li made equal contributions to this study.

[*] To whom correspondence should be addressed.

State Key Laboratory of Phytochemistry and Plant Resources in West China, Kunming Institute of Botany, Chinese Academy of Sciences, Kunming, 650201, China

E-mail: xdluo@mail.kib.ac.cn (Xiao-Dong Luo) Tel: 0871-65223177

State Key Laboratory of Respiratory Disease, National Clinical Research Center for Respiratory Disease, Guangzhou Institute of Respiratory Health, the First Affiliated Hospital of Guangzhou Medical University, Guangzhou, Guangdong, 510120, China

E-mail: zhihongjiang@gmail.com (Zhihong Jiang). Tel: 86+020-8320-5119

State Key Laboratory of Respiratory Disease, National Clinical Research Center for Respiratory Disease, Guangzhou Institute of Respiratory Health, the First Affiliated Hospital of Guangzhou Medical University, Guangzhou, Guangdong, 510120, China Tel: 86+020-8320-5119

E-mail: jeffyah@163.com (Zifeng Yang).

Abstract

Background: Alstonia scholaris is a folk medicine used to treat cough, asthma and chronic obstructive pulmonary disease in China. Total alkaloids (TA) from A. scholaris exhibit anti-inflammatory properties in acute respiratory disease, which suggests their possible anti-inflammatory effect on influenza virus infection.

Purpose: To assess the clinical use of TA by demonstrating their anti-influenza and anti-inflammatory effects and the possible mechanism underlying the effect of TA on influenza A virus (IAV) infection *in vitro* and to reveal the inhibitory effect of TA on lung immunopathology caused by IAV infection.

Methods: Antiviral and anti-inflammatory activities were assessed in Madin-Darby canine kidney (MDCK) and A549 cells and U937-derived macrophages infected with influenza A/PR/8/34 (H1N1) virus. Proinflammatory cytokine levels were measured by real-time quantitative PCR and Bio-Plex assays. The activation of innate immune signaling induced by H1N1 virus in the absence or presence of TA was detected in A549 cells by Western blot. Furthermore, mice were infected intranasally with H1N1 virus and treated with TA (50, 25 and 12.5 mg/kg/d) or oseltamivir (60 mg/kg/d) for 5 days *in vivo*. The survival rates and body weight were recorded, and the viral titer,

proinflammatory cytokine levels, innate immune cell populations and histopathological changes in the lungs were analyzed.
Results: TA significantly inhibited viral replication in A549 cells and U937-derived macrophages and markedly reduced cytokine and chemokine production at the mRNA and protein levels. Furthermore, TA blocked the activation of pattern recognition receptor (PRR)- and IFN-activated signal transduction in A549 cells. Critically, TA also increased the survival rate, reduced the viral titer, suppressed proinflammatory cytokine production and innate immune cell infiltration and improved lung histopathology in a lethal PR8 mouse model.
Conclusion: TA exhibits anti-viral and anti-inflammatory effects against IAV infection by interfering with PRR- and IFN-activated signal transduction.

Keywords: Alstonia scholaris; total alkaloids, influenza A virus; acute lung injury; anti-inflammatory; innate immune response

Abbreviations:
AMø: alveolar macrophages; Akt: protein kinase B; ARDS: acute respiratory distress syndrome; ATCC: the American Type Culture Collection; BALF: bronchoalveolar lavage fluid; CARD: caspase recruitment domain; CH25H: cholesterol 25-hydroxylase; CMC: carboxymethyl cellulose; CFDA: China Food and Drug Administration; DCs: dendritic cells; DMSO: dimethyl sulfoxide; dpi: days post infection; ERK: extracellular signal-regulated kinase; GAPDH: glyceraldehyde-3-phosphate dehydrogenase; HE: hematoxylin-eosin; HPAI: highly pathogenic avian influenza; IAV: influenza A virus; IFN: interferon; IFITMS: interferon-induced transmembrane proteins; IFNAR: interferon-α/β receptor; IFNLR: interferon-λ receptor; IL-1β: interleukin-1β; IL-6: interleukin-6; IL-8: interleukin-8; IP-10: interferon-inducible protein-10; IRF: interferon regulatory factor; ISG: interferon-stimulated gene; ISGF: interferon-stimulated gene factor; JAK-STAT: janus activated kinase-signal transducer and activator of transcription; KC: keratinocyte-derived cytokine; LD_{50}: 50% lethal dose; MAPK: extracellular signal-regulated kinase; MAVS: mitochondrial antiviral-signaling protein; MCP-1: monocyte chemoattractant protein-1; MDA-5: melanoma differentiation-associated gene-5; MDCK: Madin-Darby canine kidney; MIP-1α: macrophage inflammatory protein-1α; MIP-1β: macrophage inflammatory protein-1β; MOI, multiplicity of infection; MTT: 3-(4,5-dimethylthiazol-2-yl)-2,5-diphenyltetrazolium bromide; NAIs: neuraminidase inhibitors; IFNs: interferons; NF-κB: nuclear factor kappa-B; NK: natural killer; PMA: phorbol myristate acetate; PRRs: intrinsic cellular pattern recognition receptors; RANTES: regulated upon activation normal T cell expressed and secreted factor; RIG-I: retinoic acid-inducible gene I; TA: total alkaloids; $TCID_{50}$: 50% tissue culture infective dose; TLR: Toll-like receptor; TNF-α: tumor necrosis factor-α; TRIF: TIR-domain-containing adaptor-inducing interferon-β; TRIM: tripartite interaction motif

Introduction

Influenza A virus (IAV) is a highly contagious pathogen that causes human respiratory infections and has a significant impact on global health. Seasonal influenza virus accounts for an estimated 291,243-645,832 deaths each year (Iuliano et al., 2018). Through genetic adaptation, IAV can promote interspecies transmission from avian hosts to humans. The emblematic influenza virus subtype is H5N1 highly pathogenic avian influenza (HPAI), which has caused severe disease and high mortality rates in humans since 1997 in southern China. More recently, other HPAIs (including H5N6, H5N8 and H7N9) have emerged and pose serious threats to public health (Paul

et al., 2019; Simon et al., 2016).

Antiviral drug therapy provides direct and rapid control of influenza virus replication and has been shown to have clinical benefits. At present, FDA-approved antivirals to treat IAV include neuraminidase inhibitors (NAIs), such as oseltamivir, zanamivir and peramivir, and inhibitors of influenza cap-dependent endonuclease, such as baloxavir (Chow et al., 2019). Although the frequency of circulating influenza viruses with reduced susceptibility to NAIs is low (Takashita et al., 2020), resistant viruses are more frequently selected during NAI treatment in hospitalized children and particularly in those who are immunocompromised (Memoli et al., 2010). Furthermore, even in patients without prior baloxavir treatment, a virus with a polymerase acidic subunit I38T substitution conferring reduced susceptibility to baloxavir has been identified (Takashita et al., 2019a; Takashita et al., 2019b). In particular, worse disease outcomes of patients with influenza A(H1N1)pdm09 were found to be related to a delayed initiation of antivirals (Álvarez-Lerma et al., 2016; Rodríguez et al., 2011). Thus, alternative therapeutic strategies that can compensate for the limitations of antivirals are strongly required.

It is clear that not only the replicating competence of IAV but also a robust inflammatory response contributes to the morbidity or ultimately death caused by IAV. IAV infection drives the release of type I interferons (IFNs), proinflammatory cytokines, and chemokines from the respiratory epithelium through the activation of cellular signaling pathways, which further recruit immune cells, such as macrophages, neutrophils, monocytes and natural killer (NK) cells, to facilitate the clearance of the virus (Iwasaki and Pillai, 2014). However, in severe IAV infections, the virus induces an unrestrained inflammatory response that impairs host tolerance, resulting in tissue damage (Iwasaki and Pillai, 2014). It has been demonstrated that specific leukocytes and high levels of cytokine and chemokine expression contribute to disease severity in severe human and avian IAV infections (Karawita et al., 2019). There is also a significant correlation between acute respiratory distress syndrome (ARDS) and marked cytokine activation in pandemic H1N1 2009 IAV infections (To et al., 2010). Thus, the hyperinduction of inflammatory cytokine production, known as a "cytokine storm," is an important factor driving lung immunopathology. The use of interventions that restore the dysregulated immune response resulting in ARDS and death is therefore an indispensable therapeutic strategy to improve severe lung injury caused by IAV.

Alstonia scholaris (*Apocynaceae*) is a medicinal plant distributed in deciduous and evergreen forests and plains over tropical regions of Africa and Asia (Zhao et al., 2016). The leaves of *A. scholaris* have historically been used in China to treat chronic respiratory diseases, including cough, asthma and chronic obstructive pulmonary disease (Yang et al., 2014). We previously showed that the oral administration of total alkaloids (TA) isolated from *A. scholaris* produced inhibitory effects on leukocyte and cytokine production in response to LPS-induced airway inflammation in rats, reduced the eosinophil population and IL-4 expression and promoted IL-10 expression in the bronchoalveolar lavage fluid (BALF) of airway allergic inflammatory model mice (Zhao et al., 2017; Zhao et al., 2016). TA also downregulated inflammatory cell and cytokine production in a postinfectious cough mouse model (Zhao et al., 2018). Based on their anti-inflammatory activity, we further studied the antiviral and anti-inflammatory effects of TA in an influenza virus-induced acute lung injury mouse model and the underlying innate immune signaling mechanism upon detection of IAV infection.

Materials and methods

Preparation of TA and reference alkaloids

Leaves of *A. scholaris* were collected in May 2018 in Pu'er city, Yunnan Province, People's

Republic of China, and identified by Dr. Xiao-Dong Luo, Kunming Institute of Botany, Chinese Academy of Sciences. A voucher specimen (Luo20180501) has been deposited in the State Key Laboratory of Phytochemistry and Plant Resources in West China, Chinese Academy of Sciences. Dried and powdered leaves of *A. scholaris* were extracted with 90% EtOH under reflux conditions (3 h × 4), and the solvent was evaporated in vacuo to obtain ethanolic extract. Next, the ethanolic extract was dissolved in 0.3% aqueous HCl solution and filtered, and the residue was identified as a nonalkaloid fraction. The acidic solution was adjusted to pH 9-10 with 10% aqueous ammonia and was extracted with EtOAc to obtain a TA fraction (lot number: 180501), in which picrinine (12.3%), vallesamine (14.1%), scholaricine (3.7%), and 19-epischolaricine (0.9%) were quantified by HPLC with four standard compounds. The TA was identified by matching their high-resolution MS data with those of isolated compounds from the genus *Alstonia*. Matching scores of the identified compounds were calculated based on ion mass error, isotope space and isotope abundance. The reference compounds scholaricine (lot 20150407 purity >98%), 19-scholaricine (lot 20150407 purity >98%), vallesamine (lot 20150407, purity >98%) and picrinine (lot 20150407, purity >98%) were isolated by Luo's group and stored in a refrigerator, Kunming Institute of Botany, Chinese Academy of Sciences.

Cell lines and the virus

The human lung carcinoma A549, Madin-Darby canine kidney (MDCK) and human leukemia U937 cell lines were purchased from ATCC. A549 and MDCK cells were cultured in Dulbecco's modified Eagle's medium (DMEM, Gibco, USA) supplemented with 10% fetal bovine serum (FBS) at 37°C. The U937 cells were cultured in RPMI 1640 supplemented with 10% heat-inactivated FBS, 2.5 mM glutamine and 10 mM HEPES and differentiated into macrophages by exposure to 100 ng/mL phorbol myristate acetate (PMA; Sigma, USA) for 48 h. Influenza A/Puerto Rico/8/34 (H1N1) was obtained from ATCC and propagated in the allantoic cavities of chicken eggs.

Cytotoxicity assay

The cytotoxic effects of TA on A549 and MDCK cells and U937-derived macrophages were assessed using the MTT assay. Briefly, cells were seeded in 96-well plates for 24 h at 37°C and subsequently rinsed with PBS. The indicated concentrations of TA were then added to the cells. After 24 h of incubation, the cells were stained with MTT solution at 0.5 mg/mL for 4 h. Finally, the supernatants were removed, and the formed formazan crystals were dissolved in 200 μL of dimethyl sulfoxide (DMSO). The absorbance at 570 nm was measured with a Multiskan Spectrum reader (Thermo Fisher, USA).

In vitro antiviral assays

The cell monolayers of A549 and MDCK cells and U937-derived macrophages were exposed to H1N1 virus at a MOI of 1 for 2 h at 37°C. After the virus was adsorbed, the inoculum was removed and replaced with culture medium containing the indicated concentrations of TA, 3.5 μM oseltamivir carboxylate (Stru Chem Co., Ltd, China), 10μM dexamethasone (Sigma, USA) or DMSO for another 24 h. The culture supernatants were then collected for viral titer and cytokine measurement, and the cells were harvested for RNA isolation. The viral titer was determined by a 50% tissue culture infective dose ($TCID_{50}$) assay and calculated by the Reed-Muench method (Reed and Muench, 1938).

Reverse transcriptase PCR and real-time quantitative PCR

Total RNA isolation and qPCR were performed as previously described (Li et al., 2017). Real-time quantitative PCR was performed with TaqMan probes and primer sets using an Applied Biosystems 7500 system. The primer and probe sequences used for analysis are listed in Table S1. The relative gene expression was calculated using the $2^{-\Delta\Delta Ct}$ method with GAPDH as an internal reference.

Proinflammatory cytokine detection in the culture supernatant

The cytokine levels in the culture supernatants were measured using a Bio-Plex Pro Human Cytokine Screening Panel (Bio-Rad) according to the manufacturer's instructions. The assay plate was analyzed with a Bio-Plex Luminex 200 XYP instrument (Bio-Rad Laboratories). The data were calculated using Bio-Plex Manager software (version 5.0; Bio-Rad Laboratories).

Western blot analysis

Cells were lysed on ice for 10 min with radioimmunoprecipitation assay lysis buffer (Beyotime Institute of Biotechnology, Haimen, China) supplemented with a phosphatase inhibitor cocktail (Sigma). The protein concentration was determined with a bicinchoninic protein assay kit. Western blots were performed as previously described (Wang et al., 2018). The primary antibodies were from CST Biological Reagents Co., Ltd (Shanghai, China) against Toll-like receptor 3 (TLR-3), retinoic acid-inducible gene I (RIG-I), melanoma differentiation-associated antigen 5 (MDA-5), phospho-interferon regulatory factor 3 (p-IRF-3), IRF-3, phospho-p65(p-p65), p65, MDA-5, phospho-signal transducer and activator of transcription 1 (p-STAT1), STAT1, phospho-signal transducer and activator of transcription 2 (p-STAT2), STAT2, interferon-stimulated gene 15 (ISG-15) and GAPDH at a dilution of 1:1,000 overnight at 4°C, followed by horseradish peroxidase-conjugated secondary antibodies (CST Biological Reagents Co., Ltd) for 60 min at room temperature (RT). The protein bands were detected using a Western Lighting Chemiluminescence system (Thermo Fisher Scientific, Inc.) and quantified by ImageJ software (NIH, Bethesda, MD, USA).

Animal experiments

Female SPF C57BL/6 mice (SCXK20160002) weighing between 16 g and 18 g were obtained from Hunan SJA Laboratory Animal Co. Ltd (Hunan, China). The mice were housed in collective cages under a 12 h light/dark cycle, with free access to food and water. The air temperature was maintained at 22 ± 2°C with a relative humidity of 50 ± 10%. All animal care and experimental procedures were approved by the Animal Care and Use Committee of Guangzhou Medical University.

In the inflammation study, mice (n=32 per group) anesthetized with 2.5% isoflurane were intranasally challenged with 50 μL of virus ($5\times LD_{50}$) or PBS. TA (50, 25 and 12.5 mg/kg/d), oseltamivir phosphate (Stru Chem Co., Ltd, China) (60 mg/kg/d) or 0.5% carboxymethyl cellulose (CMC)-Na was orally administered to infected mice once daily starting from the day of infection and continuing to 5 days post infection (dpi). All mice were sacrificed by euthanasia at 4 and 6 dpi. At each time point, the BALF from 4 mice per group was collected and centrifuged at 1,100 × g for 15 min at 4°C. The supernatants were used for the subsequent detection of the viral titer and inflammatory mediator expression. The lungs from another 6 mice per group were collected at each time point for the flow cytometric analysis of innate immune cells. The lungs from the remaining mice were fixed with 10% neutral formalin for histopathological examination. For the

survival study, the body weights and death of mice (n=10 per group) were monitored daily until 15 dpi.

Proinflammatory cytokine detection in the BALF

The protein concentration in the BALF was measured using a Pierce BCA Protein Assay kit (Thermo Fisher Scientific (China) Co., Ltd) according to the manufacturer's protocol. The expression levels of cytokines and chemokines in the BALF were measured and quantified by the Bio-Plex Pro Mouse Cytokine assay using the Bio-Plex 200 Multiplex Testing System (Bio-Rad, USA) according to the manufacturer's protocol.

Flow cytometric analysis

The lungs were harvested from PBS-perfused mice and mechanically diced into small tissue pieces using surgical scissors. The diced lungs were suspended in 4 mL of digestion buffer (1 mg/mL collagenase D (Roche, UK), 0.1 mg/mL DNase I (Roche, UK), 2% FBS, 2 mM L-glutamine, 25 mM HEPES in HBSS) for 30 min at 37°C. The lungs were then disrupted mechanically through a 70 μm cell strainer, and the red blood cells were lysed using red blood cell lysis buffer (Biolegend, USA). The cell pellets were resuspended in FACS buffer, and the Fc receptors were blocked using 25 mg/mL anti-mouse CD16/32 (Biolegend, USA). The cells were stained with the following anti-mouse antibodies: GhostDye510 (TONBO Biosciences, USA), FITC anti-mouse CD3 (Biolegend, USA), PerCP/Cy5.5 anti-mouse CD45 (Biolegend, USA), Alexa Fluor® 647 anti-mouse F4/80 (Biolegend, USA), APC/Cy7 anti-mouse CD11b (Biolegend, USA), PE anti-mouse CD11c (Biolegend, USA), PerCP/Cy5.5 anti-mouse Ly6G (Biolegend, USA) and PE anti-mouse NK1.1 (Biolegend, USA). Flow cytometry acquisition was performed with BD FACSVerse^{TM} flow cytometer (Becton, Dickinson and Company, USA). The data were analyzed using FlowJo software.

Histopathological examination

Mouse lungs fixed in 10% formalin were embedded in paraffin and then cut into 4 μm-thick sections. The sections were further stained with hematoxylin-eosin (HE) and captured by light microscopy (Nikon, ECLIPSE NI-U).

Statistical analysis

Statistical analysis was performed using GraphPad Prism 7.0 software. The differences in viral titer, the mRNA and protein levels of proinflammatory cytokines, Western blot quantification and innate immune cell populations among groups were compared using one-way analysis of variance (ANOVA). The surviving mice were analyzed with the Kaplan-Meier method. A value of $p<0.05$ was considered to be statistically significant.

Results

TA alkaloids

Total indole alkaloids from *A. scholaris* were registered by Luo's group as an investigational new botanical drug (No. 2011L01436) and approved for phase I/II clinical trials by the China Food and Drug Administration (CFDA). In fact, TA alkaloidal constituents were intensively investigated by Luo's group, and as a result, more than 100 alkaloids were reported. Among our literature, 8 monoterpenoid indole alkaloids were introduced as "Hot off the press" in *Natural Products Reports*, and two of them were reviewed by the top journal *Chemical Reviews*. Moreover, 14

indole alkaloids were synthesized by outstanding chemists after we published their structures and/or bioactivities. Moreover, antitussive, anti-asthmatic and expectorant, anti-airway inflammation and protection against postinfectious cough *in vivo* were also verified by Luo's group (Shang et al., 2010; Zhao et al., 2016; Zhao et al., 2018). In addition, the chemical profile, metabolites and pharmacokinetic behaviors of TA were presented (Zhao et al., 2017), with scholaricine, 19-epischolaricine, vallesamine, and picrinine (Fig. S2) as the major leaf indole alkaloids. Recently, pharmacokinetic and safety evaluations of multiple doses of TA in healthy Chinese volunteers have been completed in a phase I clinical trial (Li et al., 2019), which supports further phase II clinical trials.

Following previous literature, qualitized TA must include quantitative determination of major bioactive alkaloids, scholaricine, 19-epischolaricine, vallesamine, and picrinine as chemical markers. In the present investigation, TA were prepared (lot number: 180501). In total, twenty-five alkaloids were identified, except for peaks No. 9 and No. 11 (Fig. 1 and Table 1). Extractive ion chromatograms (EICs) of four alkaloids (No. 10, No. 12, No. 23, No. 24) in TA and their reference standards are shown in Figure 2. The EICs and mass spectra of all twenty-seven TA alkaloids are presented in the supporting information (Fig. S1). The contents of picrinine (12.3%), vallesamine (14.1%), scholaricine (3.7%), and 19-epischolaricine (0.9%) were determined by HPLC-DAD in the supporting information (Fig. S2).

Antiviral activity of TA on IAV in vitro

The nontoxic TA concentration was determined by MTT assay in MDCK and A549 cells and U937-derived macrophages. The results showed that TA did not affect the viability of all the cell lines at concentrations up to 128 μg/mL (Fig. 3A-C). Therefore, the concentrations of TA used in the subsequent *in vitro* studies were 25, 50 and 100 μg/mL. As shown in Fig. 4A and B, the progeny viruses were markedly suppressed by TA treatment at effective concentrations of 25 to 100 μg/mL in MDCK and A549 cells. TA at 100 μg/mL exhibited a significant inhibitory effect on the progeny viruses in U937-derived macrophages (Fig. 4C).

Inhibition of IAV-induced cytokine and chemokine expression by TA in A549 cells

To determine the anti-inflammatory effect of TA on the expression of cytokines and chemokines induced by H1N1 infection, the mRNA expression levels of TNF-α, IFN-α, IFN-β, IFN-γ, IFN-λ2, IL-6, CXCL-8/IL-8, CCL-2/MCP-1, CXCL-10/IP-10, CCL-3/MIP-1α, CCL-4/MIP-1β and CCL-5/RANTES were measured after TA treatment. We found that the expression of these cytokines and chemokines was dramatically elevated at 24 h after viral infection (Fig. 5), whereas this increase was significantly inhibited by DEX (10 μM) or TA treatment (100, 50 and 25 μg/mL) (Fig. 5). Similarly, DEX or TA treatment attenuated the upregulated production of inflammatory mediators in the A549 cell supernatant (Fig. 6).

Inhibition of IAV-induced cytokine and chemokine expression by TA in U937-derived macrophages

In addition, the anti-inflammatory activity of TA was also tested in U937-derived macrophages. At concentrations of 100, 50 and 25 μg/mL, TA treatment significantly suppressed the mRNA expression of TNF-α, IL-6, CXCL-10/IP-10, IFN-α and IFN-β (Fig. 7). Moreover, it also reduced levels of IFN-α2, IFN-β, IL-1β, IL-6 and IP-10 in the macrophage culture supernatant (Fig. 8). DEX at 10 μM concentration significantly suppressed mRNA expression and protein production of these cytokines (Fig. 7-8).

Suppressive effects of TA treatment on PRR- and IFN-activated signal transduction in A549 cells

In response to IAV infection, pattern recognition receptors (PRRs) recognize viral gene segments and active transcription factors, including NF-κB and IRF-3/7, which further bind to the promotor of IFNs and induce IFN expression. IFNs activate signal transduction and induce the expression of ISGs. We found that the expression of PRRs (TLR-3, RIG-I and MDA-5) and IRF-3 was profoundly downregulated by TA treatment (Fig. 9A-D). The phosphorylation levels of p65, STAT1 and STAT2 were significantly decreased after TA treatment (Fig. 9E-G). Downstream of IFN-activated signaling, the activation of the antiviral protein ISG-15 was significantly impaired in cells incubated with TA (Fig. 9H).

Protective effects of TA treatment on IAV-infected mice

The infected mice showed symptoms including reduced activity, appetite loss and dull fur from 3 dpi and progressed to respiratory distress until death. The body weight of the infected mice began to decrease at 3 dpi and reached a minimum at 10 dpi. and increased again for those that survived to the endpoint. Treatment with 60 mg/kg/d oseltamivir and 50 mg/kg/d TA improved the symptoms and weight loss in infected mice (Fig. 10A). In the placebo group, mice began to die on day 8 dpi and presented a 30% survival rate at 15 dpi. The oral administration of oseltamivir and 50 mg/kg/d TA increased the survival rate to 100% ($p<0.01$) and 70% ($p<0.05$), respectively (Fig. 10B). Significantly lower viral titers in BALF of infected mice were observed following treatment of 60mg/kg/d oseltamivir (4 and 6dpi, $p<0.01$, $p<0.001$) or 50mg/kg/d TA (6dpi, $p<0.01$) (Fig. 10C).

Influence of TA treatment on lung inflammation in IAV-infected mice

After H1N1 infection, the cytokines whose levels peaked at 4 dpi in mouse BALF included TNF-α, IFN-α2, IFN-β, KC, MIP-1α and RANTES (Fig. 11A). We found that at this time point, TA administration significantly suppressed the production of TNF-α, IFN-α2, KC and RANTES (Fig. 11A). In addition, IFN-β, KC and MIP-1α production was also inhibited at 6 dpi in TA-treated mice (Fig. 10A). The levels of cytokines such as IFN-γ, IL-6, MCP-1, IP-10, MIP-1β and MIG peaked in the late phase (6 dpi) in H1N1-infected mice (Fig. 10A). At this time point, the levels of these cytokines were significantly reduced in mice treated with TA 50 mg/kg/d (Fig. 11A). Moreover, 50 mg/kg/d TA treatment significantly eliminated the increase in total protein levels in the BALF of infected mice (Fig. 11B).

Furthermore, we analyzed immune cell populations in mouse lungs taken from 4 and 6 dpi. The cells were stained for resident alveolar macrophages (AMø; $CD11b^{-}CD11c^{+}F4/80^{+}$), monocyte-derived Mø ($CD11b^{+}Ly6G^{-}F4/80^{+}$), neutrophils ($CD11b^{+}Ly6G^{+}$), dendritic cells (DCs; $CD11b^{+}CD11c^{+}$) and natural killer (NK) cells ($NK1.1^{+}CD3^{-}$), and the gating strategy is shown in Figure S2. Monocyte-derived AMø, neutrophils, DCs and NK cells were significantly reduced in the lungs of TA-treated mice in a dose-dependent manner at 6 dpi (Fig. 12A, C-E). We observed that the resident AMø population was continually reduced from 4 to 6 dpi, which was reversed by TA treatment at 50 mg/kg/d at 6 dpi (Fig. 12B). These results imply that TA can protect mice against IAV-induced excessive inflammatory responses in the lungs.

We next examined the histopathologic changes in the lungs of the mice. At 4 dpi, neutrophil infiltration was found in the bronchial lumen of the placebo control mice (Fig. 13B). The peribronchial epithelium showed mild lymphocyte infiltration (Fig. 13B). The pulmonary tissues adjacent to bronchioles showed thickened walls with mild lymphocytic inflammation and a small number of AMø in the lumen (Fig. 13B). At 6 dpi, the lesion severity increased, and the lesions

extended to an increased range of lung tissues, characterized by multifocal lymphocytic infiltration (Fig. 13H). As expected, TA treatment significantly reduced inflammatory cell infiltration in a dose-dependent manner (Fig. 13D-F, J-L).

Discussion

Human influenza H1N1 virus infection causes a wide range of disease severity, from asymptomatic to severe febrile respiratory symptoms. In most cases, IAV infection is self-limiting. However, in populations at the extremes of age or with a compromised immune system or other underlying health conditions, IAV can establish fulminant pneumonia and rapidly progress to ARDS (Hendrickson and Matthay, 2013; Pulendran and Maddur, 2015; Ramsey and Kumar, 2011). Despite great progress in the development of anti-influenza agents, morbidity and mortality remain high. The factors contributing to severe lethality include the loss of the protective host innate immune response mediated by excessive localized immune cell recruitment and inflammatory mediator release, which occurs at the late stage of infection when the virus is almost eliminated by antiviral therapy. It has been demonstrated that severe cases of influenza A (H1N1) pdm09 infection produce excessive cytokine and chemokine responses (Thomas et al., 2017). Leukocytosis and increased C-reactive protein, cytokine and chemokine levels are often observed in severe pediatric patients infected with the influenza A (H1N1) pdm09 virus (Kim et al., 2011; Matsumoto et al., 2012; Okada et al., 2011). Therefore, more research is needed for the development of interventions targeting uncontrolled lung inflammation.

In severe IAV infection, the virus productively replicates in respiratory epithelial cells, the primary target, leading to the release of type I/II IFNs to promote the antiviral response and various inflammatory mediators, including chemokines CCL3/MIP-1α, CCL2/MCP-1 and CCL5/RANTES, which recruit monocytes, as well as CXCL-1/KC (IL-8 in humans), which attract neutrophils to the infected site (Lamichhane and Samarasinghe, 2019). Monocytes and neutrophils initiate an early response by releasing proinflammatory cytokines, including TNF-α, IL-1, IL-6, and type I and II IFNs, which further recruit immune cells, resulting in excessive inflammation (Tang et al., 2019). Upon recognition of virus-infected cells, Møs produce a panel of key proinflammatory cytokines associated with lung injury (Tang et al., 2019). However, animal studies have shown aggravated disease severity following IAV infection after complete removal of lung neutrophils or Mø (Cardani et al., 2017; Tate et al., 2009). NK cells contribute to lethal pathology in high-dose IAV infections but protect mice from lower-dose infections (Zhou et al., 2013). The same disparate mechanism also exists for lung DCs, which are required for initiating CD8+ T cell responses to augment viral clearance but are also responsible for secreting inflammatory mediators, a possible role in recruiting other leukocytes (Ho et al., 2011). Therefore, therapeutically regulating rather than completely abrogating the innate immune response is considered to be a logical strategy in treating IAV infection. In our study, we first showed that TA strongly reduced the expression of a diverse set of proinflammatory cytokines *in vitro* and *in vivo*. TA treatment was further demonstrated to partially reduce the recruitment of lung monocytes, neutrophils, monocyte-derived Mø, NK cells and DCs accompanying lethal H1N1 infection without impairing innate immune cells developed in the respiratory system. IAV infection can lead to resident AMø depletion, establishing a niche for secondary infection (Ghoneim et al., 2013). TA effectively reversed the resident AMø depletion, suggestive of a restoration in pulmonary innate immunity to prevent further bacterial superinfections. Altogether, our observations suggest that TA treatment improves disease outcome by fine-tuning the cytokine storm and innate immune cell development in lungs from H1N1-infected mice.

Intrinsic cellular PRRs, such as RIG-I, MDA-5 and TLRs, play a central role in signal transduction, which mounts innate antiviral and inflammatory responses for the control of IAV infection. RIG-I, MDA-5 and TLR-3 specifically sense nucleic acids or intermediates formed during IAV replication (Chow et al., 2018). Upon recognition, the CARD domains of RIG-I and MDA-5 interact with the MAVS protein in mitochondrial membranes (Kasumba et al., 2017). In contrast, TLR-3 activates TRIF, whereas TLR- 4, 7, 8, and 9 recruit the adaptor Myd88 (Biondo et al., 2019). Activated MAVS and TRIF induce the coordinated activation of NF-κB and IRF-3, which leads to the release of proinflammatory cytokines (TNF-α, IL-1β, IL-6, etc.) and IFNs (type I, IFN-α and IFN-β; type II, IFN-γ; type III, IFN-λ) (Biondo et al., 2019; Chen et al., 2018). Accumulating evidence has revealed that RIG-I and TLR-3 play protective roles in IAV-infected hosts by orchestrating IFN-dependent antiviral responses. The administration of a synthetic RIG-I agonist before IAV infection can reduce the viral titer and enhance death protection in mice (Chiang et al., 2015). Another study showed that natural-origin RIG-I ligand quickly increases the expression of IFN and a panel of cytokines and chemokines in mouse lungs by activating TLR-3 and MDA-5, resulting in the downregulation of viral replication (Kasumba et al., 2017). In contrast, TLR-3 may contribute to pathology in severe disease since mice deficient in TLR-3 are protected against infection by HPAI H5N1 and lethal H3N2 viruses (Huo et al., 2018; Le Goffic et al., 2006; Leung et al., 2014). It has also been reported that the upregulation of RIG-I is closely associated with the enhanced cytokine response during H5N1 infection (Hui et al., 2011). In the present study, TA at 100 μg/mL showed inhibitory activity toward RIG-I and MDA-5 as determined in A549 cells infected with H1N1 virus. In addition, TA treatment at this dose suppressed TLR-3 expression, with the expression of TLR-7 and Myd88 remaining unchanged (data not shown). The phosphorylation of p65, the NF-κB transcription factor, and IRF-3 was also significantly dampened by TA treatment. Following the robust release of IFNs, an interaction between IFN, IFNAR and IFNLR occurs, which activates JAK-STAT signaling. Phosphorylated STAT1 and STAT2 coupled with IRF9 form ISGF3, which translocate to the nucleus and triggers a range of ISGs followed by the synthesis of antiviral proteins, such as the Mx family proteins, IFITMS, CH25H, TRIM and ISG-15 (Chen et al., 2018). Upon treatment with 100 μg/mL TA, the levels of p-STAT1, p-STAT2 and ISG-15 were markedly decreased. A variety of signaling pathways, such as the Raf/MEK/ERK, NF-κB, PI3K/Akt/mTOR and p38 MAPK pathways, are indispensable for IAV replication (Choi et al., 2016; Planz, 2013). Our results show that TA treatment does not inhibit the phosphorylation-induced activation of p-ERK 1/2, p-Akt and p-p38 in H1N1-infected A549 cells (data not shown). Notably, although TA treatment suppressed IFN synthesis and did not impair various pathways supporting viral replication, the viral titer was still decreased according to *in vitro* and *in vivo* studies, providing hints at the underlying mechanism of viral factors. Together, our results indicate that TA show inhibitory activity toward a wide range of molecules involved in the RIG-I-, MDA-5- and TLR3-dependent signaling cascades encoding IFN and subsequent pathways activated by the IFN system (Fig. 14, schematic diagram). IAV infection activates the IFN signaling pathway induced by PRR sensing. TA treatment downregulates TLR-3, RIG-I, MDA-5 and IRF-3 activity and inhibits the phosphorylation of p65, STAT1 and STAT2 and the expression of downstream ISG-15 in A549 cells.

Conclusion

In summary, we demonstrate that TA display anti-influenza and anti-inflammatory effects by interfering with PRR- and IFN-activated signal transduction. The results of this study provide evidence that TA may potentially be used as an anti-inflammatory treatment strategy in

IAV-infected patients.

Conflict of interest

All authors declare that there are no conflicts of interest.

Acknowledgments

This work was supported by the National Key Research and Development Program of China (2017YFC1704007), the Key Projects of Dongguan City Social Science and Technology Development Plan (Grant/Award Number: 2018507150011645), the Science and Technology Development Fund in Macao Special Administrative Region (Grant no. 125/2017/A3) and the Science Research Project of Guangdong Province (Grant no. 2019B121205010).

Supplementary materials

Supplementary material associated with this article can be found in the online version.

References

Álvarez-Lerma, F., Marín-Corral, J., Vila, C., Masclans, J.R., de Molina, F.J.G., Loeches, I.M., Barbadillo, S., Rodríguez, A & on behalf of the H1N1 GETGAG/SEMICYUC Study Group., 2016. Delay in diagnosis of influenza A (H1N1) pdm09 virus infection in critically ill patients and impact on clinical outcome. Crit Care 20, 337.

Biondo, C., Lentini, G., Beninati, C., Teti, G., 2019. The dual role of innate immunity during influenza. Biomed J 42, 8-18.

Cardani, A., Boulton, A., Kim, T.S., Braciale, T.J., 2017. Alveolar Macrophages Prevent Lethal. Influenza Pneumonia By Inhibiting Infection Of Type-1 Alveolar Epithelial Cells. PLoS Pathog 13, e1006140.

Chen, X., Liu, S., Goraya, M.U., Maarouf, M., Huang, S., Chen, J.-L., 2018. Host Immune Response. to Influenza A Virus Infection. Front Immunol 9, 320.

Chiang, C., Beljanski, V., Yin, K., Olagnier, D., Yebdri, F.B., Steel, C., Goulet, M.-L., DeFilippis, V.R., Streblow, D.N., Elias K, S., Haddad, E.K., Trautmann, L., Ted. R., Hiscott, J, 2015. Sequence-Specific Modifications Enhance the Broad-Spectrum Antiviral Response Activated by RIG-I Agonists. J Virol 89, 8011-8025.

Choi, M., Heo, J., Yi, C., Ban, J., Lee, N., Lee, N., Kim, S., Kim, N., Inn, K., 2016. A novel p38. mitogen activated protein kinase (MAPK) specific inhibitor suppresses respiratory syncytial virus and influenza A virus replication by inhibiting virus-induced p38 MAPK activation. Biochem Biophys Res Commun 477, 311-316.

Chow, E.J., Doyle, J.D., Uyeki, T.M., 2019. Influenza virus-related critical illness: prevention, diagnosis, treatment. Crit Care 23, 214.

Chow, K., Gale Jr, M., Loo, Y., 2018. RIG-I and Other RNA Sensors in Antiviral Immunity. Annu Rev Immunol 36, 667-694.

Ghoneim, H.E., Thomas, P.G., McCullers, J.A., 2013. Depletion of alveolar macrophages during influenza infection facilitates bacterial super-infections. J Immunol 191, 1250-1259.

Hendrickson, C.M., Matthay, M.A., 2013. Viral Pathogens and Acute Lung Injury: Investigations. Inspired by the SARS Epidemic and the 2009 H1N1 Influenza Pandemic, Seminars in respiratory and critical care medicine. Semin Respir Crit Care Med 34, 475-486.

Ho, A., Prabhu, N., Betts, R., Ge, M., Dai, X., Hutchinson, P., Lew, F., Wong, K., Hanson, B., Macary, P., 2011. Lung CD103+ dendritic cells efficiently transport influenza virus to the

lymph node and load viral antigen onto MHC class I for presentation to CD8 T cells. J Immunol 187, 6011-6021.

Hui, K., Lee, S., Cheung, C., Mao, H., Lai, A., Chan, R., Chan, M., Tu, W., Guan, Y., Lau, Y., 2011. H5N1 influenza virus-induced mediators upregulate RIG-I in uninfected cells by paracrine effects contributing to amplified cytokine cascades. J Infect Dis 204, 1866-1878.

Huo, C., Jin, Y., Zou, S., Qi, P., Xiao, J., Tian, H., Wang, M., Hu, Y., 2018. Lethal influenza A virus preferentially activates TLR3 and triggers a severe inflammatory response. Virus Res 257, 102-112.

Iuliano, A.D., Roguski, K.M., Chang, H.H., Muscatello, D.J., Palekar, R., Tempia, S., Cohen, C., Gran, J.M., Schanzer, D., Cowling, B.J., 2018. Estimates of global seasonal influenza-associated respiratory mortality: a modelling study. Lancet 391, 1285-1300.

Iwasaki, A., Pillai, P.S., 2014. Innate immunity to influenza virus infection. Nat Rev Immunol 14, 315-328.

Karawita, A., Tong, M., Short, K., 2019. A delicate balancing act: immunity and immunopathology in human H7N9. influenza virus infections. Curr Opin Infect Dis 32, 191-195.

Kasumba, D., Hajake, T., Oh, S., Kotenko, S., Kato, H., Fujita, T., 2017. A Plant-Derived Nucleic Acid Reconciles Type I IFN and a Pyroptotic-like Event in Immunity against Respiratory Viruses. J Immunol 199, 2460-2474.

Kim, Y., Kim, J., Hyun, M., 2011. Cytokine response in pediatric patients with pandemic influenza H1N1. 2009 virus infection and pneumonia: comparison with pediatric pneumonia without H1N1 2009 infection. Pediatr Pulmonol 46, 1233-1239.

NF-κB: nuclear factor kappa-B;

Lamichhane, P.P., Samarasinghe, A.E., 2019. The Role of Innate Leukocytes during Influenza Virus Infection. J Immunol Res 2019, 8028725.

Le Goffic, R., Balloy, V., Lagranderie, M., Alexopoulou, L., Escriou, N., Flavell, R., Chignard, M., Si-Tahar, M., 2006. Detrimental contribution of the Toll-like receptor (TLR) 3 to influenza A. virus–induced acute pneumonia. PLoS Pathog 2, e53.

Leung, Y.C., Nicholls, J.M., Ho, C.K., Sia, S.F., Mok, C.K., Valkenburg, S.A., Cheung, P., Hui, K.P., Chan, R.W., Guan, Y., 2014. Highly pathogenic avian influenza A H5N1 and pandemic H1N1 virus. infections have different phenotypes in Toll-like receptor 3 knockout mice. J Gen Virol 95, 1870-1879.

Li, R., Zi, M., Gou, Z., Zhao, Y., Zhang, W., Lu, F., Cao, W., Zhao, Y., Li, Q., Zhao, Y., 2019. Pharmacokinetics and safety evaluation in healthy Chinese volunteers of. alkaloids from leaf of Alstonia scholaris: A multiple doses phase I clinical trial. Phytomedicine. 61, 152828.

Li, Z., Li, L., Zhou, H., Zeng, L., Chen, T., Chen, Q., Zhou, B., Wang, Y., Chen, Q., Hu, P., 2017. Radix isatidis Polysaccharides Inhibit Influenza a Virus and Influenza A Virus-Induced Inflammation via Suppression of Host TLR3 Signaling In Vitro. Molecules 22, 116.

Matsumoto, Y., Kawamura, Y., Nakai, H., Sugata, K., Yoshikawa, A., Ihira, M., Ohashi, M., Kato, T., Yoshikawa, T., et al., 2012. Cytokine and chemokine responses in pediatric patients with severe pneumonia associated with pandemic A/H1N1/2009 influenza virus. Microbiol Immunol 56, 651-655.

Memoli, M.J., Hrabal, R.J., Hassantoufighi, A., Eichelberger, M.C., Taubenberger, J.K., 2010. Rapid Selection of Oseltamivir and Peramivir Resistant Pandemic H1N1. During Therapy in Two Immunocompromised Hosts. Clin Infect Dis 50, 1252-1255.

Okada, T., Morozumi, M., Matsubara, K., Komiyama, O., Ubukata, K., Takahashi, T., Iwata., 2011.

554 Characteristic findings of pediatric inpatients with pandemic (H1N1) 2009. virus infection
555 among severe and nonsevere illnesses. J Infect Chemother 17, 238-245.
556 Paul, M.C., Vergne, T., Mulatti, P., Tiensin, T., Iglesias, I., 2019. Editorial: Epidemiology of Avian
557 Influenza Viruses. Front Vet Sci 6, 150.
558 Planz, O., 2013. Development of cellular signaling pathway inhibitors as new antivirals against.
559 influenza. Antiviral Res 98, 457-468.
560 Pulendran, B., Maddur, M.S., 2015. Innate Immune Sensing and Response to Influenza. Curr Top
561 Microbiol Immunol 386, 23-71.
562 Ramsey, C., Kumar, A., 2011. H1N1: viral pneumonia as a cause of acute respiratory distress.
563 syndrome. Curr Opin Crit Care 17, 64-71.
564 Reed, L.J., Muench, H.A., 1938. A simple method for estimating fifty percent endpoints. Am. J.
565 Hyg. 27, 493-497.
566 Rodríguez, A., Díaz, E., Martín-Loeches, I., Sandiumenge, A., Canadell, L., Díaz, J., Figueira, J.,
567 Marques, A., Alvarez-Lerma, F., Vallés., 2011. Impact of early oseltamivir treatment on
568 outcome in critically ill patients with 2009 pandemic influenza A. J Antimicrob Chemother
569 66, 1140-1149.
570 Shang, J., Cai, X., Zhao, Y., Feng, T., Luo, X., 2010. Pharmacological evaluation of Alstonia
571 scholaris: anti-tussive, anti-asthmatic and expectorant activities. J Ethnopharmacol 129,
572 293-298.
573 Simon, P.F., de La Vega, M.-A., Paradis, É., Mendoza, E., Coombs, K.M., Kobasa, D.,
574 Beauchemin, C.A., 2016. Avian influenza viruses that cause highly virulent infections in
575 humans exhibit distinct replicative properties in contrast to human H1N1 viruses. Sci Rep 6,
576 24154.
577 Takashita, E., Daniels, R., Fujisaki, S., Gregory, V., Gubareva, L., Huang, W., Hurt, A., Lackenby,
578 A., Nguyen, H., Pereyaslov, D., 2020. Global update on the susceptibilities of human
579 influenza viruses to. neuraminidase inhibitors and the cap-dependent endonuclease inhibitor
580 baloxavir, 2017-2018. Antiviral Res 175, 104718.
581 Takashita, E., Ichikawa, M., Morita, H., Ogawa, R., Fujisaki, S., Shirakura, M., Miura, H.,
582 Nakamura, K., Kishida, N., Kuwahara, T., Sugawara, H., Sato, A., Akimoto, M., Mitamura, K,
583 Abe, T., Yamazaki, M., Watanabe, S., Hasegawa, H., Odagiri, T., 2019a. Human-to-human
584 transmission of influenza A (H3N2) virus with reduced susceptibility to baloxavir, Japan,
585 February 2019. Emerg Infect Dis 25, 2108-2111.
586 Takashita, E., Ichikawa, M., Morita, H., Ogawa, R., Fujisaki, S., Shirakura, M., Miura, H.,
587 Nakamura, K., Kishida, N., Kuwahara, T., Sugawara, H., Sato, A., Akimoto, M., Mitamura, K,
588 Abe, T., Yamazaki, M., Watanabe, S., Hasegawa, H., Odagiri, T., 2019b. Influenza A (H3N2)
589 virus exhibiting reduced susceptibility to baloxavir. due to a polymerase acidic subunit I38T
590 substitution detected from a hospitalised child without prior baloxavir treatment, Japan,
591 January 2019. Euro Surveill 24, 1900170.
592 Tang, B., Feng, C., McLean, A., 2019. Understanding the role of host response in influenza
593 pneumonitis. Intensive Care Med 45, 1012-1014.
594 Tate, M., Deng, Y., Jones, J., Anderson, G., Brooks, A., Reading, P., 2009. Neutrophils ameliorate
595 lung injury and the development of severe disease. during influenza infection. J Immunol 183,
596 7441-7450.
597 Thomas, M., Mani, R., Philip, M., Adhikary, R., Joshi, S., Revadi, S., Buggi, S., Desai, A.,
598 Vasanthapuram, R., 2017. Proinflammatory chemokines are major mediators of exuberant
599 immune response associated with Influenza A (H1N1) pdm09 virus infection. J Med Virol 89,

1373-1381.

To, K., Hung, I., Li, I., Lee, K., Koo, C., Yan, W., Liu, R., Ho, K., Chu, K., Watt, C., 2010. Delayed clearance of viral load and marked cytokine activation in severe cases. of pandemic H1N1 2009 influenza virus infection. Clin Infect Dis 50, 850-859.

Wang, Y., Li, J., Yan, W., Chen, Q., Jiang, Z., Zhang, R., Pan, X., Wang, X., 2018. An active component containing pterodontic acid and pterodondiol isolated from Laggera pterodonta inhibits influenza A virus infection through the TLR7/MyD88/TRAF6/NF‐κB signaling pathway. Mol Med Rep 18, 523-531.

Yang, X.-W., Qin, X.-J., Zhao, Y.-L., Lunga, P.K., Li, X.-N., Jiang, S.-Z., Cheng, G.-G., Liu, Y.-P., Luo, X.-D., 2014. Alstolactines A–C, novel monoterpenoid indole alkaloids from Alstonia. scholaris. Tetrahedron letters 55, 4593-4596.

Zhao, Y., Cao, J., Shang, J., Liu, Y., Khan, A., Wang, H., Qian, Y., Liu, L., Ye, M., Luo, X., 2017. Airways antiallergic effect and pharmacokinetics of alkaloids from Alstonia scholaris. Phytomedicine 27, 63-72.

Zhao, Y., Shang, J., Pu, S., Wang, H., Wang, B., Liu, L., Liu, Y., Shen, H., Luo, X., 2016. Effect of total alkaloids from Alstonia scholaris on airway inflammation in. rats. J Ethnopharmacol 178, 258-265.

Zhao, Y., Yang, Z., Shang, J., Huang, W., Wang, B., Wei, X., Khan, A., Yuan, Z., Liu, Y., Wang, Y., 2018. Effects of indole alkaloids from leaf of Alstonia scholaris on post-infectious cough in mice. J Ethnopharmacol 218, 69-75.

Zhou, G., Juang, S., Kane, K., 2013. NK cells exacerbate the pathology of influenza virus infection in mice. Eur J Immunol 43, 929-938.

623 Figure 1

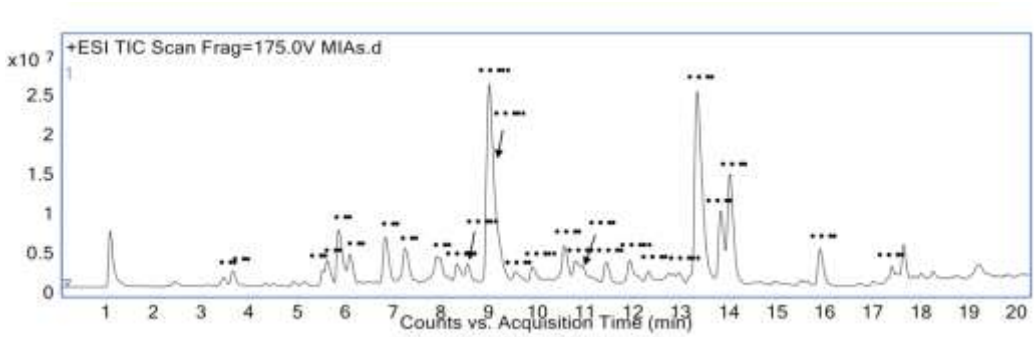

624

625 Figure 2

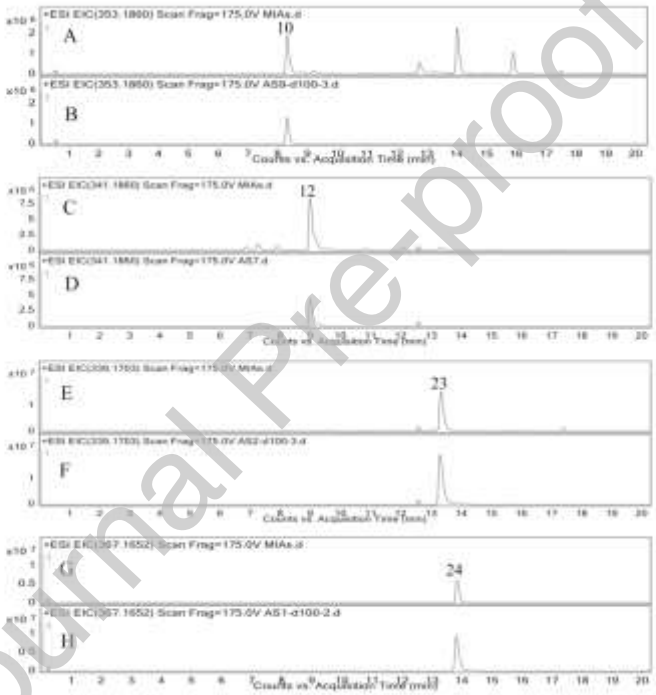

626

627

628

629

630

631

632

633

634

635

636

637

638

639

640

641

642 Figure 3

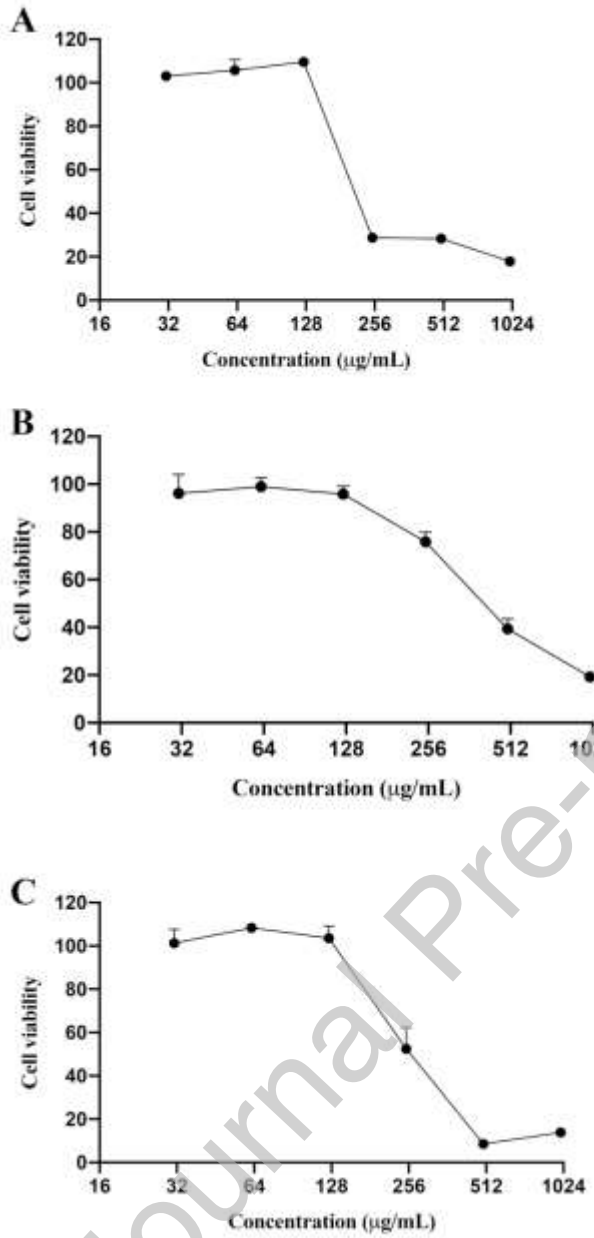

643

644

645 Figure 4

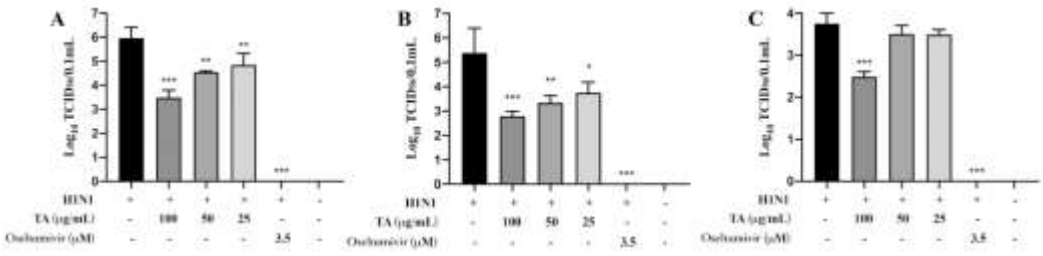

646

647

Figure 5

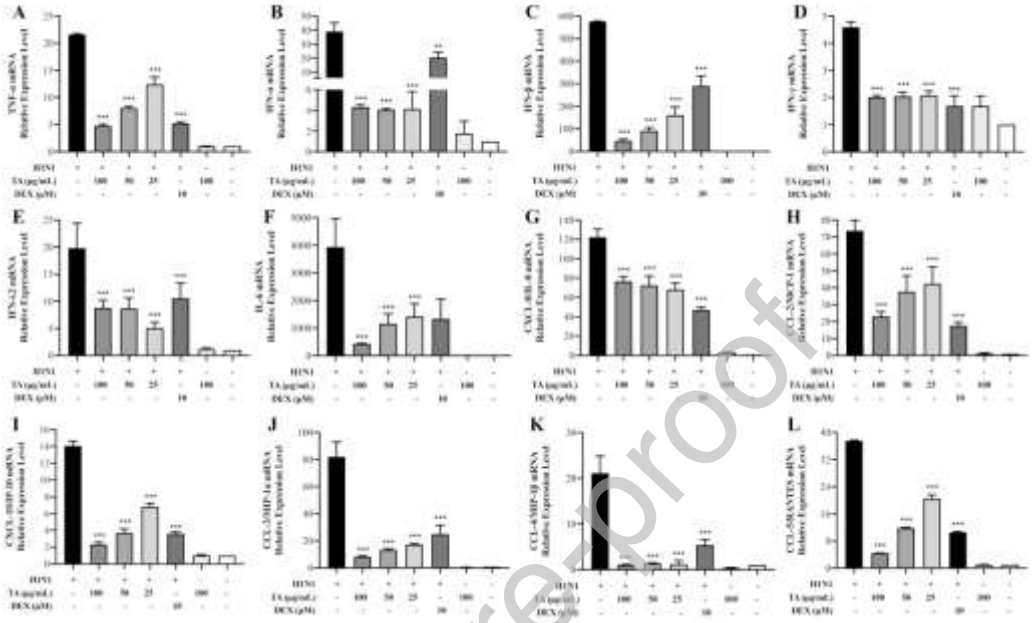

Figure 6

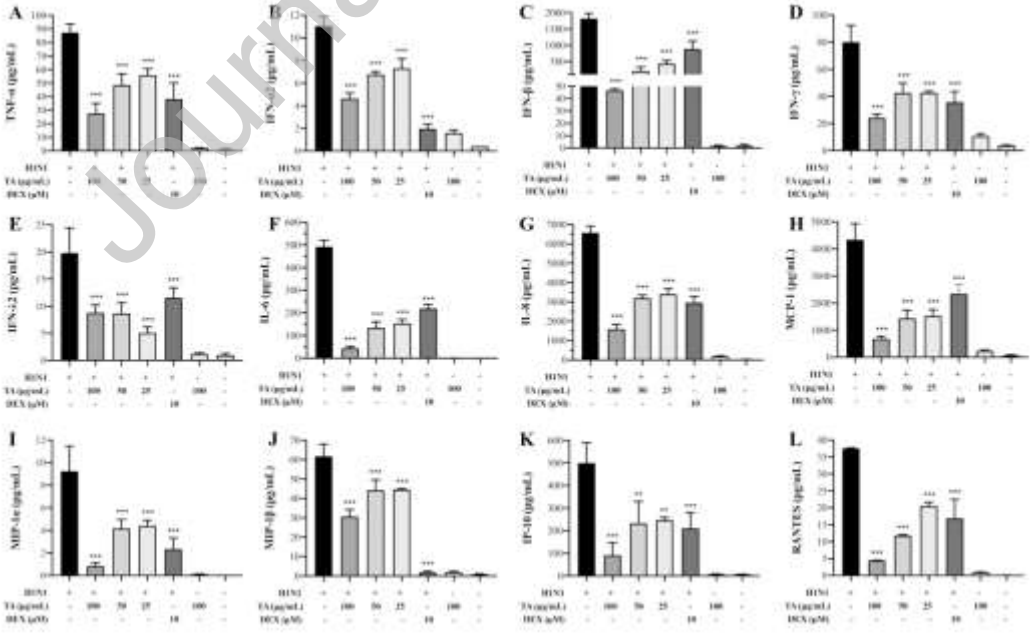

656

657

658

659

660

661

662

663

664 Figure 7

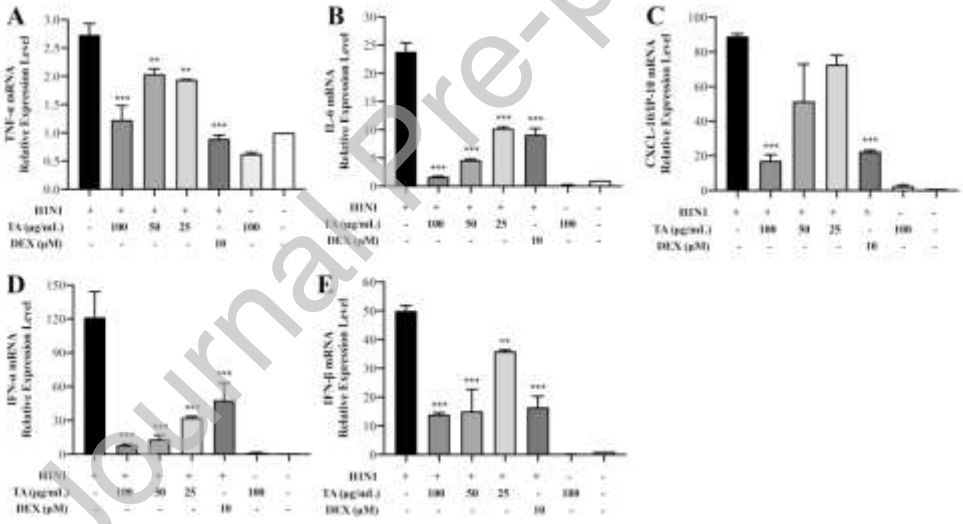

665

666

667 Figure 8

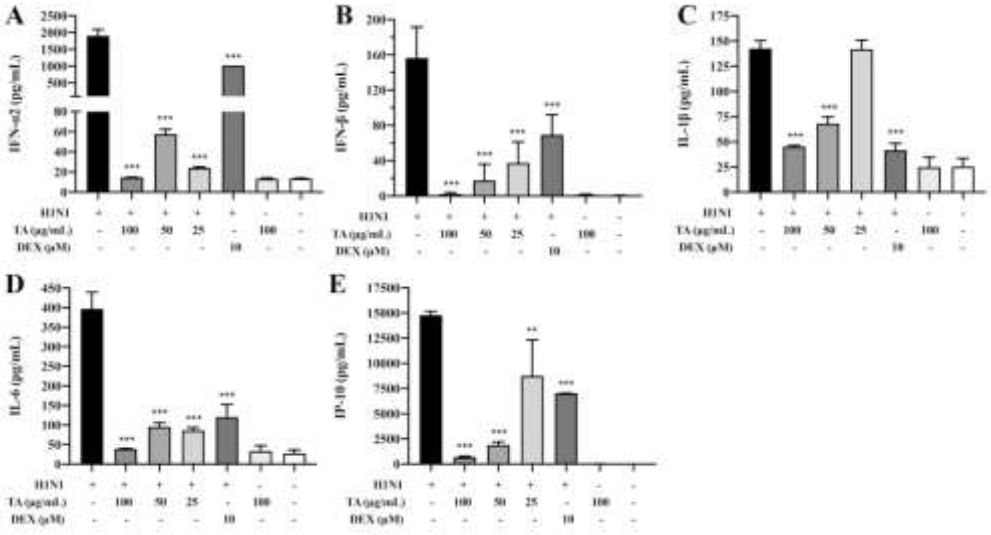

668

669

670 Figure 9

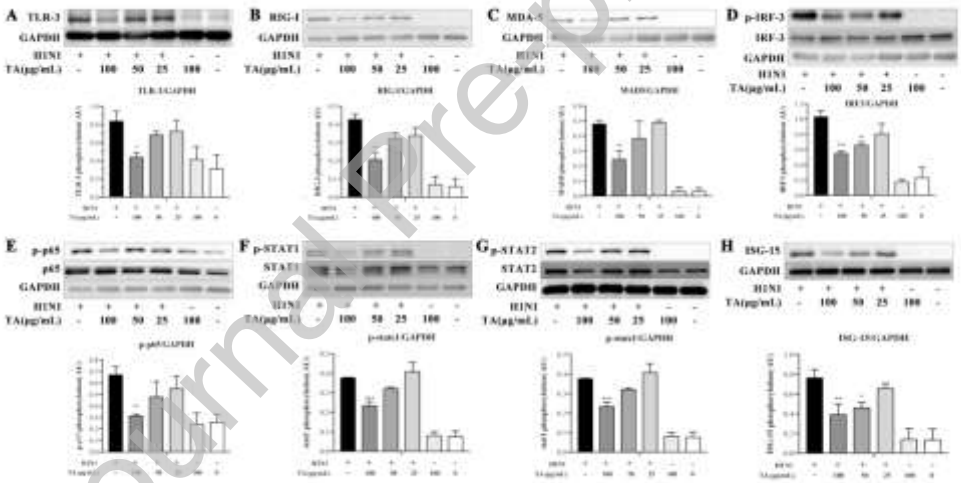

671

672

673 Figure 10

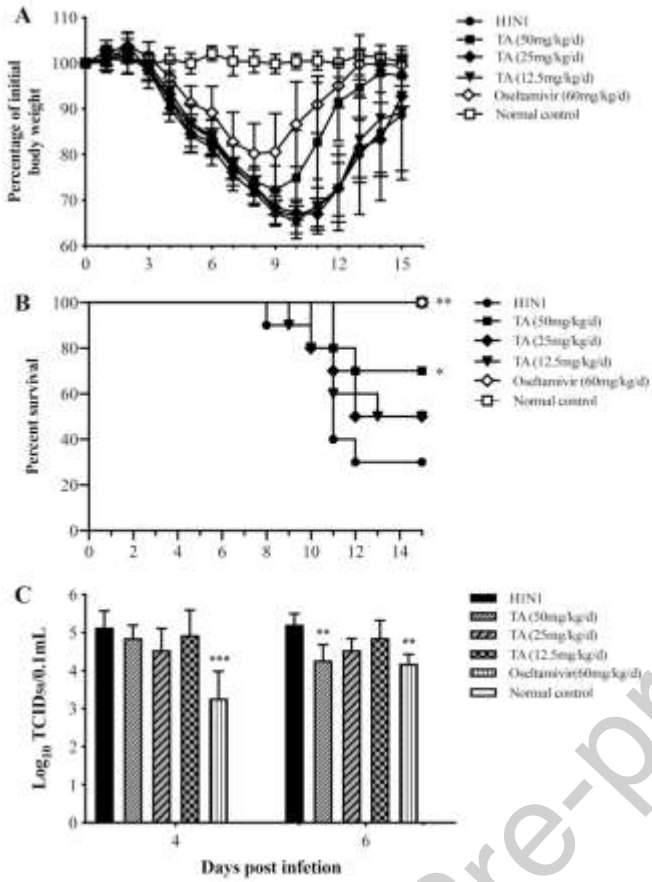

674

675

676 Figure 11

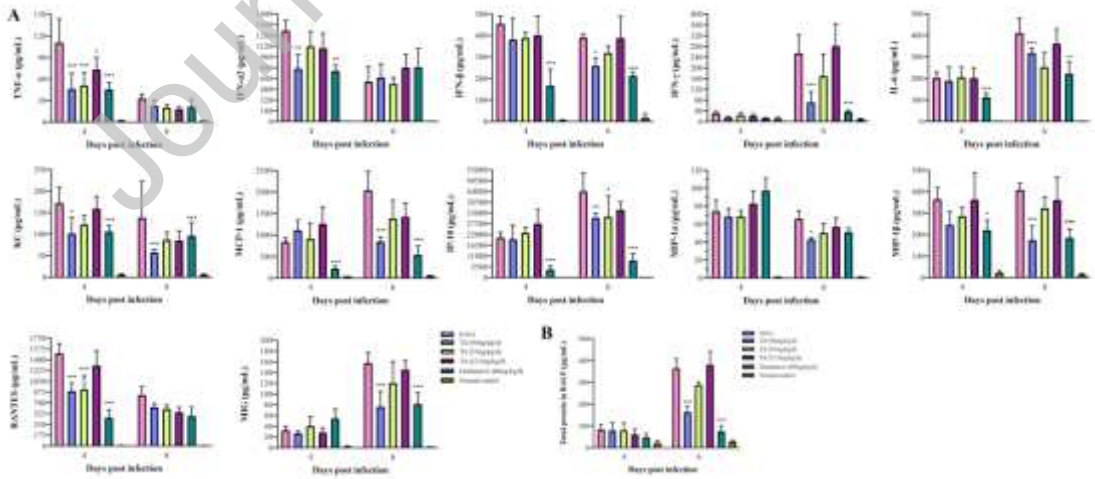

677

678

679 Figure 12

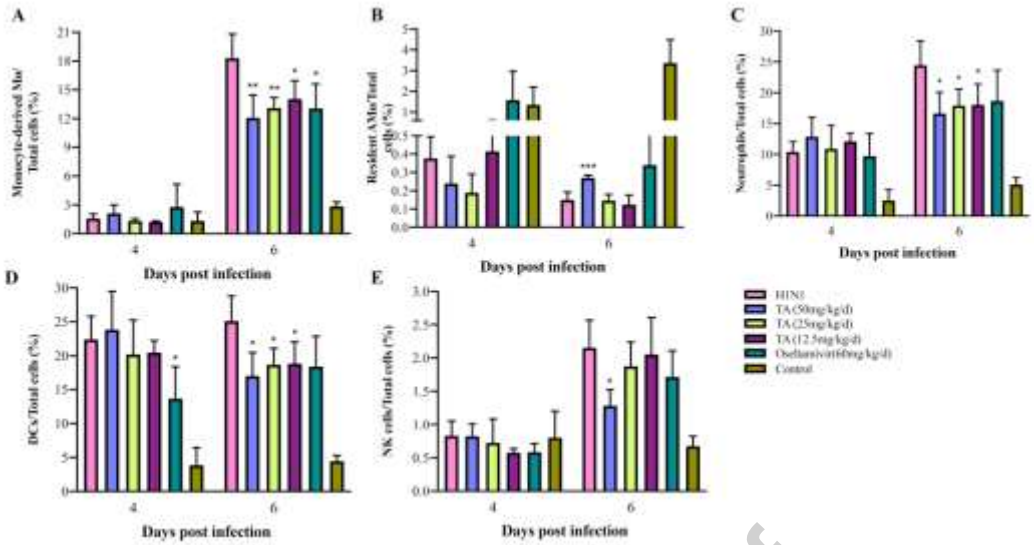

680

681

682 Figure 13

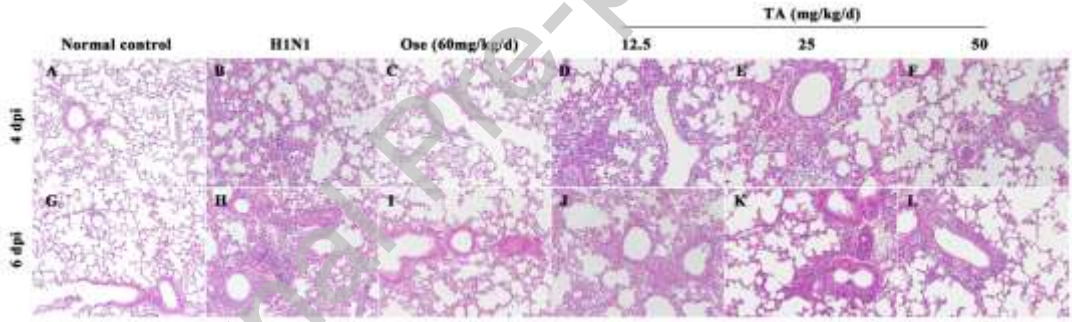

683

684

685

686

687

688

689 Figure 14

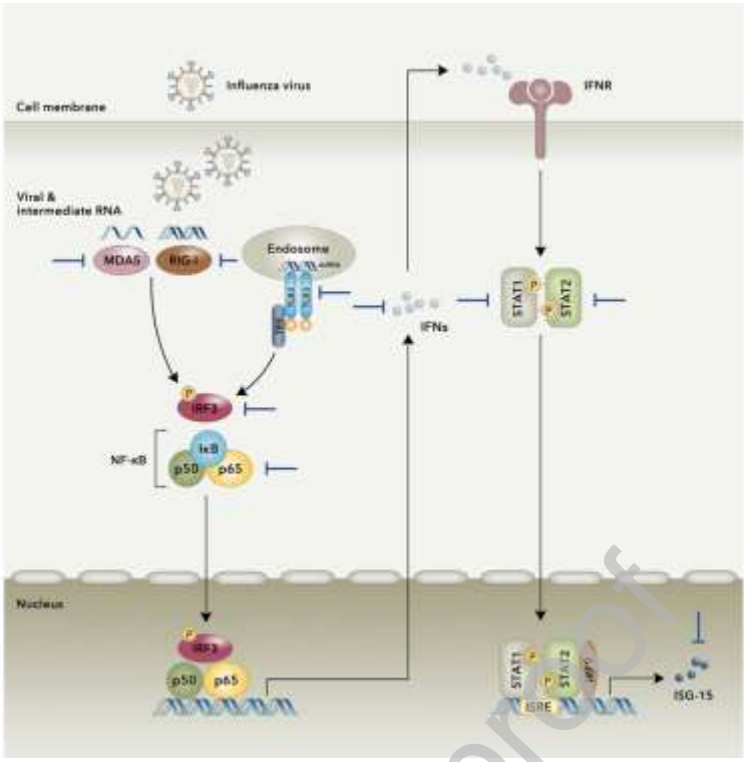

690

691

692 **Fig. 1. Total ion chromatogram (TIC) profile of TA.** Twenty-seven alkaloids are
693 labeled as peaks No. 1~No. 27.
694
695 **Fig. 2. Extractive ion chromatograms (EICs) of peaks (No. 10, No. 12, No. 23, No.**
696 **24) in TA (A, C, E, G) and reference standards (B-akuammidine, D-vallesamine,**
697 **F-picrinine, H-picralinal).** Calculated mass-to-charge ratios of the reference
698 standards corresponding to peaks (No. 10, No. 12, No. 23, No. 24) are m/z 353.1860,
699 m/z 341.1860, m/z 339.1703, and m/z 367.1652, respectively.
700
701 **Fig. 3. Cytotoxic effect of the TA on cells.** A: MDCK cells, B: A549 cells, C:
702 U937-derived macrophages. Data are presented as the mean±SD. The experiments
703 were performed in triplicate.
704
705 **Fig. 4. Inhibitory effect of TA treatment on IAV replication *in vitro*.** A: MDCK
706 cells, B: A549 cells, C: U937-derived macrophages. Oseltamivir carboxylate (3.5μM)
707 was used as a positive control. The experiments were performed in triplicate. Data are
708 presented as the mean±SD from three separate experiments. *$p < 0.05$; **$p < 0.01$;
709 ***$p < 0.001$, compared with H1N1-infected cells.
710
711 **Fig. 5. Effects of TA treatment on the mRNA expression levels of inflammatory mediators in**
712 **IAV-infected A549 cells.** A: TNF-α, B: IFN-α, C: IFN-β, D: IFN-γ, E: IFN-λ2, F: IL-6, G:
713 CXCL-8/IL-8, H: CCL-2/MCP-1, I: CXCL-10/IP-10, J: CCL-3/MIP-1α, K: CCL-4/MIP-1β, L:

CCL-5/RANTES. DEX: dexamethasone. Data are presented as the mean±SD of three separate experiments. *$p < 0.05$; **$p < 0.01$; ***$p < 0.001$, compared with H1N1-infected cells.

Fig. 6. Effects of TA treatment on the expression levels of inflammatory mediators in the supernatant of IAV-infected A549 cells. A: TNF-α, B: IFN-α2, C: IFN-β, D: IFN-γ, E: IFN-λ2, F: IL-6, G: IL-8, H: MCP-1, I: MIP-1α, J: MIP-1β, K: IP-10, L: RANTES. DEX: dexamethasone. Data are presented as the mean±SD of three separate experiments. *$p < 0.05$; **$p < 0.01$; ***$p < 0.001$, compared with H1N1-infected cells.

Fig. 7. Effects of TA treatment on the mRNA expression levels of inflammatory mediators in IAV-infected U937-derived macrophages. A: TNF-α, B: IL-6, C: CXCL-10/IP-10, D: IFN-α, E: IFN-β. DEX: dexamethasone. Data are presented as the mean±SD of three separate experiments. *$p < 0.05$; **$p < 0.01$; ***$p < 0.001$, compared with H1N1-infected cells.

Fig. 8. Effects of TA treatment on the expression levels of inflammatory mediators in the supernatant of IAV-infected U937-derived macrophages. A: IFN-α2, B: IFN-β, C: IL-1β, D: IL-6, E: IP-10. DEX: dexamethasone. Data are presented as the mean±SD of three separate experiments. *$p < 0.05$; **$p < 0.01$; ***$p < 0.001$, compared with H1N1-infected cells.

Fig. 9. Inhibitory effect of TA treatment on innate immune signaling in IAV-infected A549 cells. Quantification of each protein was performed using ImageJ. A: TLR-3, B: RIG-I, C: MDA-5, D: p-IRF-3, E: p-p65, F: p-STAT1, G: p-STAT2, H: ISG-15. Data are presented as the mean±SD of three separate experiments. *$p < 0.05$; **$p < 0.01$; ***$p < 0.001$, compared with H1N1-infected cells.

Fig. 10. Effects of TA treatment on body weight (A), mortality (B) and pulmonary viral load (C) in IAV-infected mice. Oseltamivir phosphate (60 mg/kg/d) and 0.5% CMC-Na were given to infected mice as positive and viral controls, respectively. Data in A and C are presented as the mean±SD (n=10 for A, and n=4 for C). Data in B were analyzed using the log-rank test for each group (n=10). *$p<0.05$; **$p<0.01$; ***$p<0.001$, compared with the H1N1-infected group.

Fig. 11. Effect of TA treatment on the expression levels of inflammatory mediators (A) and total protein concentration (B) in the BALF of AIV-infected mice. Data are presented as the mean±SD (n=4), *$p< 0.05$; **$p< 0.01$; ***$p< 0.001$, compared with the H1N1-infected group.

Fig. 12. Flow cytometric analysis of innate immune cells in mouse lungs. A: monocyte-derived **Møs/total cells, B: resident AMøs/total cells,** C: neutrophils/total cells, D: DCs/total cells, E: NK

cells/total cells. Data are presented as the mean±SD (n=6). *p<0.05, **p <0.01, ***p<0.001, compared with the H1N1-infected group.

Fig. 13. Histopathologic changes in mouse lung tissues stained with HE. Each group of representative images was selected from 6 mice at 4 and 6dpi. Ose: Oseltamivir phosphate (60 mg/kg/d). Original magnification: ×200.

Fig. 14. Schematic diagram of the mechanism by which TA treatment attenuates influenza H1N1 virus pathogenesis *in vitro*. Influenza H1N1 virus infection activates the IFN signaling pathway induced by PRR sensing. TA treatment downregulates TLR-3, RIG-I, MDA-5 and p-IRF-3 activity and inhibits p-p65, p-STAT1 and p-STAT2 and expression of downstream ISG-15 in A549 cells.

Table 1 Identification of alkaloids

No.	Formula	Compound name	Observed	Score	Error (ppm)	Reference
1	$C_{20}H_{24}N_2O_4$	alstoniascholarine H	357.1808	95.0	1.2	Qin, 2015
2	$C_{19}H_{22}N_2O_4$	alstoniascholarine B	343.1650	84.3	1.1	Qin, 2015
3	$C_{21}H_{26}N_2O_4$	scholaricine	371.1955	91.3	3.6	Jain, 1981
4	$C_{21}H_{26}N_2O_4$	isomer of peak 3	371.1963	99.3	0.6	
5	$C_{20}H_{24}N_2O_4$	isomer of peak 1	357.1793	93.0	4.3	
6	$C_{20}H_{24}N_2O_4$	isomer of peak 1	357.1796	95.0	3.6	
7	$C_{19}H_{22}N_2O_3$	alstoniascholarine A	327.1693	95.0	3.4	Qin, 2015
8	$C_{20}H_{24}N_2O_3$	alstoniascholarine K	341.1879	94.9	3.2	Qin, 2015
9	$C_{21}H_{28}N_2O_4$	unknown	373.2106	93.2	4.2	
10*	$C_{21}H_{24}N_2O_3$	akuammidine	353.1851	97.0	2.2	
11	$C_{22}H_{30}N_2O_4$	unknown	387.2262	90.8	4.6	
12*	$C_{20}H_{24}N_2O_3$	vallesamine	341.1864	97.9	1.1	
13	$C_{21}H_{26}N_2O_3$	scholarisine V	355.2023	97.6	2.2	Yu, 2018
14	$C_{20}H_{22}N_2O_3$	vinervine	339.1697	82.8	2.4	Cao, 2016
15	$C_{21}H_{26}N_2O_3$	isomer of Peak 13	355.2008	87.2	2.3	
16	$C_{20}H_{24}N_2O_4$	isomer of Peak 1	357.1798	96.6	2.9	
17	$C_{19}H_{20}N_2O_2$	17-nor-excelsinidine	309.1588	94.7	3.9	Zhang, 2014
18	$C_{22}H_{26}N_2O_5$	N-formylscholarine	399.1908	97.7	1.6	Jain, 2009
19	$C_{20}H_{22}N_2O_2$	akuammicine	323.1746	96.7	2.8	Boonchuay,
20	$C_{21}H_{26}N_2O_3$	isomer of Peak 13	355.2002	91.3	4.4	
21	$C_{21}H_{26}N_2O_3$	isomer of Peak 13	355.2008	92.1	0.8	
22	$C_{19}H_{22}N_2O_3$	isomer of Peak 7	327.1695	84.0	2.6	
23*	$C_{20}H_{22}N_2O_3$	picrinine	339.1713	95.7	2.9	
24*	$C_{21}H_{22}N_2O_4$	picralinal	367.1637	94.3	3.8	
25	$C_{22}H_{28}N_2O_4$	echitamine	385.2130	97.8	2.2	Qin, 2015

26	$C_{22}H_{28}N_2O_4$	isomer of Peak 25	385.2112	96.4	2.9
27	$C_{20}H_{22}N_2O_3$	isomer of Peak 14	339.1696	98.2	2.2

*Identification was confirmed by using the reference standards.

Graphical Abstract